Ultrasonics 96 (2019) 253–260

Contents lists available at ScienceDirect

Ultrasonics

journal homepage: www.elsevier.com/locate/ultras

Monitoring cleaning cycles of fouled ducts using ultrasonic coda wave interferometry (CWI)

B. Chen[a], D. Callens[a], P. Campistron[a], E. Moulin[a,*], P. Debreyne[b], G. Delaplace[b]

[a] IEMN UMR-CNRS 8520, Département Opto-Acousto-Electronique, 59313 Valenciennes, France
[b] INRA UR638, Processus aux Interfaces et Hygiène des Matériaux, BP 20039, 59651 Villeneuve d'Ascq, France

ARTICLE INFO

Keywords:
Ultrasonic
Coda wave interferometry
Fouling
Cleaning

ABSTRACT

Fouling in heat exchangers is the buildup of deposits on the solid surfaces. These deposits reduce the eco-efficiency of the processing equipment and increase the risk of subsequent surface contamination with the formation of biofilms. In the agro-food and water supplier sectors, which are our main concern, fouling on the hot walls of processing heat exchangers is a common occurrence and requires frequent cleaning cycles to ensure hygiene requirements are met. This results in a considerable ecological footprint. Sensors and diagnostic tools for monitoring fouling are thus of utmost importance to ensure the rational validation of the cleaning end-point and to decrease the environmental impact of the cleaning cycles.

In this paper, a non-destructive ultrasonic monitoring technique using coda waves and the associated signal processing was tested to monitor the evolution over time of a deposit layer on a solid wall during cleaning. To ascertain the feasibility of the method, a piece of wax of controlled thickness was deposited to simulate the initial fouling state and a cleaning cycle was launched. The decorrelation coefficient was used as an indicator to monitor fouling. This article presents the principle of this unprecedented technique for measuring the degree of fouling.

The results of the experiments show that this non-destructive monitoring technology is sensitive to changes in fouling and that the decorrelation coefficient curves are in agreement with the cleaning kinetics captured using a video camera, thus ascertaining the pertinence of the diagnostic tool proposed.

1. Introduction

Fouling in heat exchangers is generally defined as the unwanted formation of thermally insulating materials or deposits from process fluids on heat transfer surfaces [1].

Fouling leads to a rise in energy costs due to an increase in the thermal (and mechanical) energy required to overcome the additional heat transfer resistance (and pressure drop) induced by the presence of the deposit. The decrease in heat transfer due to fouling leads to oversized heat exchangers and/or energy losses. For example, in the food sector, fouling deposit formation on the surface of heat exchangers arising from the thermal treatment of foodstuffs, including pasteurization or ultra-high temperature processing of egg and milk products for sanitization, is still a major industrial problem. It requires frequent, drastic, and expensive cleaning measures to avoid any risk of contamination, thus resulting in the excessive use of rinsing water and harsh chemicals (sodium hydroxide and hydrochloric acid solutions).

Cleaning processes are often highly automated and use cleaning in place (CIP). In the food sector, cleaning takes several hours and thus constitutes a large proportion of the total production time. In the dairy and egg products industry, plant downtime allocated to CIP ranges from 4 to 6 h per day. This also means that supplementary investments are required (additional, oversized heat exchangers for food processing, cleaning lines, and additional maintenance costs…).

Nowadays, the major drawback of fouling in the dairy sector with regards eco-efficiency is not only the excess energy used but also the amount of water and detergent used in the cleaning procedures (Australia, source: Eco-efficiency manual for the Dairy Processing Industry, UNEP working group for Cleaner Production in the Food Industry, Aug. 2004). Cleaning generates excess effluent, which significantly contributes to the environmental footprint of the plant. Cleaning operations account for 50 to 90% of the wastewater sent to the wastewater treatment plant. This represents between 0.5 L and 5 L of water per liter of processed milk regardless of the type and size of the plant or equipment [2]. NIZO food research [3] attributes 80% of production costs to the consequences of fouling and cleaning in the

* Corresponding author.
E-mail address: Emmanuel.Moulin@uphf.fr (E. Moulin).

https://doi.org/10.1016/j.ultras.2018.12.011
Received 20 March 2018; Received in revised form 16 October 2018; Accepted 21 December 2018
Available online 23 December 2018
0041-624X/

dairy industry.

In the food industry, cleaning processes are frequently used but rarely optimized [4].

Nowadays, the eco-efficiency and improvement of these cycles is a challenge with a high economic impact. Beyond the sanitary and economic impacts, environmental and social concerns are no longer negligible. Even in Europe, water availability is a limiting factor for further economic development. European consumers have embraced the environmental value of products; they increasingly want to be sure that the food they consume is not only safe, healthy and affordable but also meets the highest levels of environmental considerations and sustainability. This growing awareness of environmental issues in society is largely supported by several initiatives launched at national (France, UK, Germany) and European (Food Sustainable Consumption and Production Roundtable 2009–2011) levels to assess the environmental footprint of individual foods and unit operations.

It is widely recognized that CIP can be rationalized through the online and offline use of sensors and rational indicators to reduce operating times, as well as effluent volume and load [5]. Currently, it is still very difficult to validate the cleaning end-point in the food industry, as equipment is generally sealed off and opaque. Consequently, optical methods are often impossible to use. Moreover, despite the numerous methods of detecting fouling in heat exchangers reported [6,7], most of them present drawbacks with regards the accurate monitoring of the evolution of fouling during the cleaning process and the optimization of the cleaning cycles.

Fouling can be quantified using experimental or numerical methods.

The following experimental methods are the most common: measurement of the pressure drop [6] and the mass flow of hot and cold fluids, determination of heat transfer parameters (e.g. heat transfer coefficient and thermal resistance) [8,9], direct monitoring of variations in heat flux using sensors [10–12], measurement of changes in electrical parameters (electrical resistance or conductivity) [10], fluid dynamic gauging (FDG) [13,14], and acoustic methods.

An ultrasonic sensor [15] is installed on the outer surface of a substrate to detect fouling on the other side (process side). The acoustic parameters change when fouling occurs and can be measured in transmission (one transducer as a transmitter, one as a receiver) and in pulse-echo mode (one transducer as a transmitter and receiver). The acoustic properties of fouling deposits are different from the processed liquid, so the formation of deposits will change the characteristic acoustic impedance of the medium, the time of flight, and the reflection coefficient at the interface. Echo energy is also another physical variable that changes when fouling occurs because of changes in the reflection/transmission and attenuation coefficients. Thus, damping and signal attenuation can be also used. Changes in these parameters can be an indicator of fouling deposits [16]. Ultrasound tests can be divided into two groups, those based on vibration resonance [17] and those based on ultrasound propagation. Ultrasonic guided waves are an efficient method of detecting fouling in pipes [18–20]. However, a very low frequency is required to adapt to the equipment and the test specimen. In this case, a small deposit is hard to detect. Concerning ultrasound propagation-based tests, ultrasonic guided wave methods [19,20] and acoustic impact techniques [21–23] have been primarily used to detect fouling formation. Among the acoustic impact techniques, a Mechatronic Surface Sensor (MSS) has been developed to monitor deposits inside a pipe using the vibration properties of surface waves such as the amplitude and damping factor [22,23]. These methods are not very sensitive yet, especially for thin layers. The decay of echo energy is also used to detect fouling. This method can detect the presence of layers 800 μm thick, but the irregularity of fouling such as an irregular surface could increase the error of the results.

As far as numerical methods are concerned, a heat exchanger is considered as a system. First, a model is developed including the parameters presented in real heat exchangers and the inputs/outputs of the model are studied continuously to provide an indication of the degree of fouling. There are two main approaches: (i) to compare the outputs of a model fed with real data with the outputs of the actual system [24]; (ii) to continuously adapt the model to the inputs/outputs and to analyze the variations in the model parameters. Whichever approach is considered, the degree of fouling can be assessed by analyzing the variation in the model parameters or by differentiating the estimated outputs from the actual outputs (analysis of the residuals). Different models have been developed based on various principles: Kalman filters [25], Fuzzy observers [26], Linear Parameter-Varying (LPV) systems [27], Subspace-based identification techniques [28], Neural networks, and nonlinear regressors [29]. Unfortunately, they only provide a global indication of the degree of fouling and have rarely been tested in real fouling conditions. Most of these models are “grey box” models, i.e. the structure and/or model parameters are motivated by prior knowledge about the physical behavior of the heat exchanger. This explains why their set-up and the work to ascertain their validity in real fouling situations are time-consuming. The computational load is sometimes an additional obstacle to implementing these detection methods in systems for monitoring fouling in real time.

According to a survey of online methods available for monitoring fouling, the most common drawbacks of existing tools are reliability, significance and ease of interpretation of the information contained in the indicator (local fouling representing the local thickness of the hot wall layer or global fouling representing the state of fouling in the entire heat exchanger), as well as sensitivity to thin layers, invasiveness, time to establish the fouling diagnosis, computational load for easy inclusion in any supervision software, and simplicity of the device for measuring the degree of fouling including set-up, tuning and maintenance stages, robustness, and economic cost.

Fortunately, of course, fouling diagnostic tools can sometimes provide total satisfaction depending on the applications. Nevertheless, the detection of local thin deposits and tiny changes in the deposits in real time is still a challenge to be overcome. Some methods are not sensitive enough to describe small changes that occur at the interface and others need special conditions or equipment, which are not always compatible with actual applications.

In industry, having a non-invasive, online, fast, reliable, robust, and inexpensive method to monitor fouling is essential. In addition, the analysis and signal processing systems must be simple and the fouling detection methods must be very sensitive. Unfortunately, this is not currently the case and consequently, the cleaning cycles are frequently unsupervised. Industrial CIP procedures currently rely on practical experience with excessive safety margins in terms of duration and environmental footprint, but this situation is no longer acceptable. Tools must be proposed to enable the online diagnosis of fouling to help the decision-making process and revamp the cleaning cycles based on rational knowledge.

One major issue is to avoid placing fouling sensors on the process side (in the bulk or on the inner surface of the heat exchanger in contact with the processed fluid). Industrials are often reluctant to use sensors in direct contact with the products being processed as this may result in additional hygiene problems and false positives since fouling strongly depends on the substrate. Therefore, this should be definitively avoided in the food industry. Moreover, embedded sensors would not have a long service life with such severe online operating conditions (temperature, shear stress due to flow rate, chemical agents).

The aim of this contribution is to help resolve this issue. In this paper, non-destructive ultrasonic monitoring technique using coda waves is presented. Acoustic wave signals can be divided into 3 parts: ballistic waves, coda waves, and noise. Ballistic waves are the first to arrive and propagate directly from the source to the sensor. Coda waves are the latter part of the signal and have a small amplitude. The noise is the part after the coda waves and is much attenuated. Coda waves are strongly scattered in the test specimen, so it is difficult to analyze the paths of each wave in the same way as direct waves [30]. However, coda waves propagate multiple times in the specimen, which means the

information they carry is much more sensitive than that of direct waves [31–33].

Recently, coda waves have been used in numerous domains such as seismic monitoring [34–36] and concrete monitoring [37–41]. These studies show an excellent sensitivity to changes in the specimen. To date and to our knowledge, coda waves have not yet been used to monitor changes in fouling deposits. This article proposes to use a highly sensitive technique to monitor fouling using ultrasonic coda waves called coda wave interferometry (CWI). The principle of CWI is to compare the initial state with other perturbed states. By analyzing the difference between the coda waves at different instants, it is possible to predict changes in deposits. Consequently, the continuous measurement of fouling is possible.

First, the theory of CWI is briefly reminded. Then, the protocol of the experiments conducted in controlled fouling and cleaning conditions, including the instruments and the operating conditions, is detailed. The difference between the monitoring results with and without wax is then discussed.

2. Materials and method

2.1. Principle of the ultrasonic coda waves method

2.1.1. Description of coda waves

As evoked in the introduction, acoustic signals can be measured experimentally to study the information in the specimen (medium in which fouling layer is to be characterized). These acoustic signals can be divided into three parts: direct waves, coda waves, and noise. Coda waves are the latter part of the signal after the direct waves. Direct waves propagate directly from the source to the sensor (Fig. 1) whereas coda waves are strongly scattered in the medium and decay more slowly than direct waves (Fig. 1). Since coda waves propagate multiple times in the medium, they are much more sensitive to any changes than direct waves. Coda waves are a combination of waves that propagate along numerous paths and are difficult to separate. However, they are not random. If there is no change in the medium, there will be no change in the path of each scattered wave either. Conversely, if the medium is disrupted, the paths of the scattered waves will change. Experimentally, a reference signal, which generally corresponds to an initial state, is measured. The signal is then measured after disruption of the medium and compared with the reference signal. Small changes in the medium result in few differences in the direct waves (Fig. 2(b)). However, the differences in the coda waves are obvious (Fig. 2(c)). Therefore, the evolution of a specimen can be monitored with good sensitivity by analyzing the evolution of coda waves at different times.

2.1.2. Calculation of the decorrelation coefficient

Most of the acoustic parameters frequently used such as time-of-flight and reflection coefficients, are difficult to extract from coda waves. An indicator representing the global change in coda waves is therefore proposed to analyze the information carried by the coda. This indicator is called the decorrelation coefficient and represents the degree of dissimilarity between two signals. The decorrelation coefficient is given by equation (1).

$$D_{1,2} = 1 - \frac{\boldsymbol{r}_{s1,s2}(0)}{\sqrt{\boldsymbol{r}_{s1,s1}(0)\boldsymbol{r}_{s2,s2}(0)}} \quad (1)$$

where s_1 is the reference signal in a given specimen state; s_2 is the signal of a subsequent perturbed state.

$r_{s1,s2}(0)$is the cross-correlation coefficient of s_1, s_2 at zero lapse-time and $r_{s1,s1}(0)$ and $r_{s2,s2}(0)$ are the auto-correlation coefficients of s_1 and s_2, respectively, with no shift.

In our application, s_1 and s_2 are specific time-windowed, band-pass filtered parts of the whole signal. It is commonly accepted that a time window of width ΔT that is at least 10 times the period corresponding to the excitation frequency is appropriate [42]. In order to describe correctly the frequency content in these time-windowed signals, the filtering frequency range Δf must satisfy the classical condition $\Delta f > 1/\Delta T$ [43].

The aim of the denominator is to normalize the inter-correlation coefficient between -1 and 1, so the decorrelation coefficient is within the interval [0, 2]. The smaller the decorrelation coefficient, the fewer changes appear in the medium. Conversely, higher decorrelation coefficients correspond to substantial changes.

2.2. Protocol for monitoring deposit cleaning

2.2.1. Presentation of the cleaning loop and positioning of the fouling deposit

In the experiment, a wax layer of controlled thickness was used to represent the industrial deposit in a cleaning loop (Figs. 3 and 4) comprising two parts: a water bath and a rectangular duct made of stainless steel and measuring 51.5 cm * 11 cm * 0.8 cm. The top plate of the duct, which could be opened, was used as the substrate on which the wax layer was placed. Wax was chosen here as the fouling material essentially for practical reasons: it is soft, cheap, and easy to obtain. It melts easily when heated and solidifies when cooled. A piece of wax can be placed on a clean substrate by solidifying liquid wax; the shape is easy to control mechanically during or after the solidification step.

The piece of wax was placed on the inner surface of the substrate as follows: after cleaning the substrate surface with alcohol and acetone, a rectangular stencil consisting of a hole measuring 6 cm by 3.2 cm in a metallic plate 6 mm thick was put on the substrate and filled with liquid wax. After several minutes, the wax solidified and the stencil was removed leaving a 6-mm thick rectangular piece of wax on the substrate. This represented the initial fouling state.

A water bath was used to heat the water and keep the cleaning water circulating inside the duct at a fixed temperature (70 °C here). The water flow was about 16 ml/s. The average circulation velocity was 18 mm/s. The bath and the duct were connected by hosepipes. The input and output temperatures were monitored using thermometers installed at both extremities of the duct. The cleaning process was monitored using acoustic sensors to show the feasibility of the CWI method as detailed below.

The signal acquisition system consisted of a laptop computer, an amplifier, an acoustic generator (Function/Arbitrary Waveform Generators, Keysight 33600A Series), a USB acquisition board (PicoScope 5000 Series), and two sensors (one for measuring the cleaning and the other used as a control) glued to the outer surface of

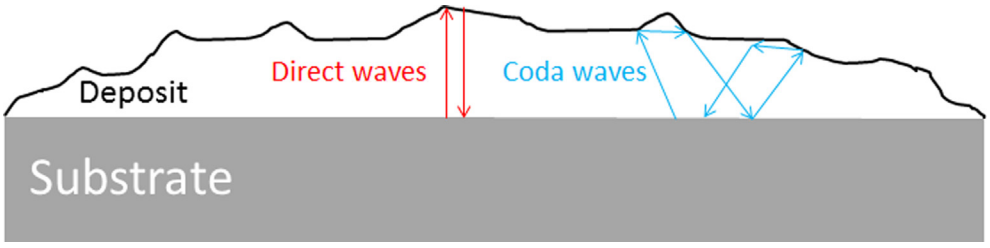

Fig. 1. schematic diagram of the propagation paths of direct waves and coda waves.

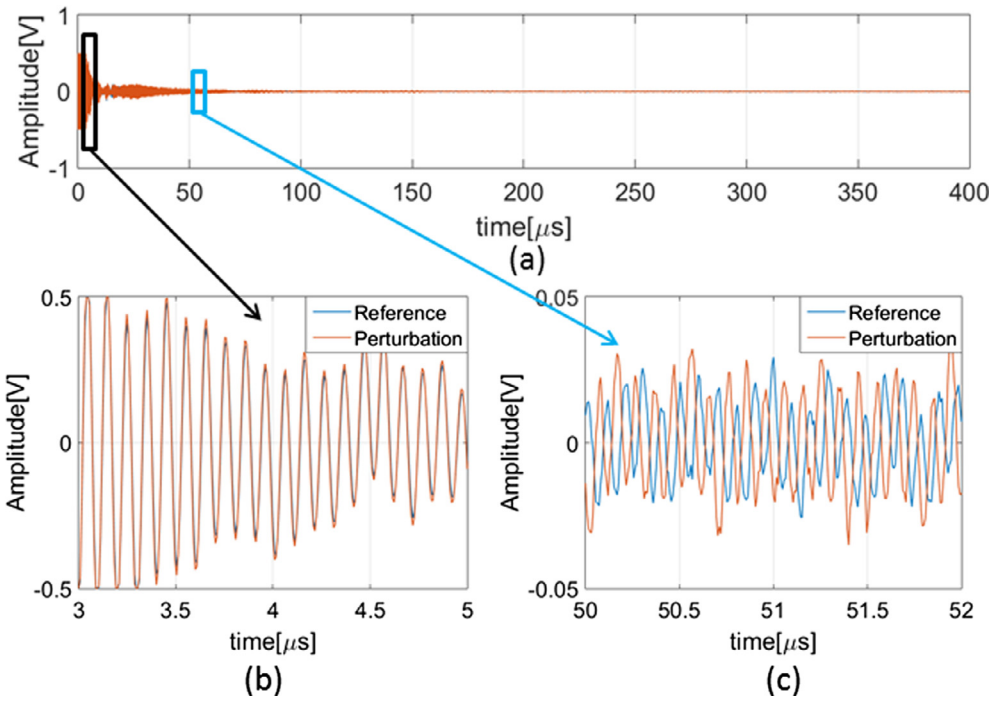

Fig. 2. Evolution over time of the amplitude of two ultrasonic signals (a) and two zoomed plots showing specific time slots (b) and (c). (a) Perturbation signal (red) and reference signal (blue), which is hidden behind the perturbation signal. The time range for the two signals is (0–400 μs); (b) The part of the direct waves in the signal (3–5 μs) where the reference signal and the perturbation signal coincide; (c) The part of coda waves in the signal (50–52 μs) where the difference between the reference signal and the perturbation signal is obvious.

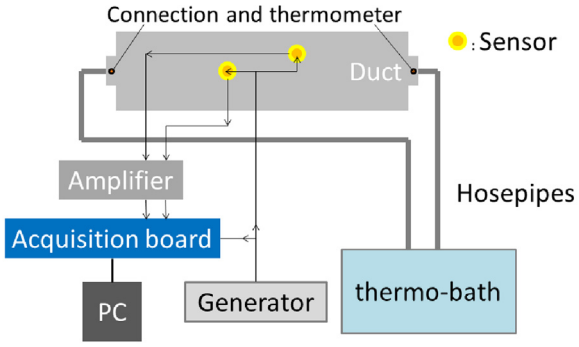

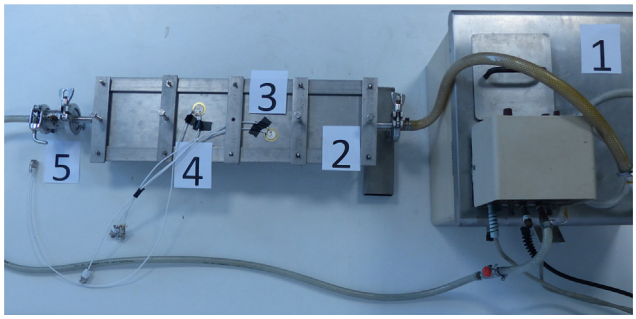

Fig. 3. Diagram of the monitoring system (top); Photo of the cleaning system (bottom), 1: water bath; 2: duct; 3: measurement sensor with wax; 4: control sensor without wax; 5: connection of duct and hosepipe with thermometer.

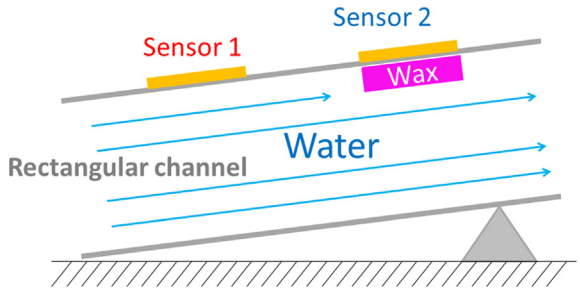

Fig. 4. Diagram detailing the inside and the outside of the duct. The hot water flows through the duct from left to right. A small support is placed under the right side of the duct to create a slight angle. Sensor 2 measures the evolution of the wax in the cleaning system. Sensor 1 records the data without wax as a control.

the duct using a strong adhesive. The sensors used in the experiment were piezoelectric transducers consisting of two concentric active parts (Fig. 5). The active inner part was for emission (ultrasound source). The other part was for acquisition (receiver). The generator created a pulsed signal of one sinusoid period that was sent to the emission transducers. The source transducer converted the electrical signal to an acoustic signal, which was emitted into the substrate. The acoustic waves propagated, reflected, and scattered inside the substrate, the deposit, and the duct. Part of these waves was intercepted by the receiving transducer and recorded using the acquisition board. There are 3 channels of acquisition board used in the experiment: one was used to monitor the source signal from the generator, and two were used to receive the signals from the sensors. The sampling frequency was 125 MHz. The amplifier was connected between the acquisition board and the sensors to amplify the signals received and filter out any low-frequency noise caused by the vibration of the support. The signal data in the acquisition board was transmitted to the PC for further processing (Fig. 3).

2.2.2. *The cleaning protocol*

The duct was cleaned with alcohol before each measurement. The wax was placed on the inner surface of the duct beneath sensor 2 (Fig. 4). The physical parameters of the paraffin wax used were as follows: density 900 kg/m^3; Young's modulus 61.4 MPa; sound velocity 1300 m/s. After installing the wax, the duct was sealed and inserted in the water circulation loop at a slight angle and the cleaning process was started. This angle was designed to help the water flow and rapidly expel any air bubbles remaining in the duct. The temperature of the water bath was set to 70 °C. Simultaneously, the acquisition system

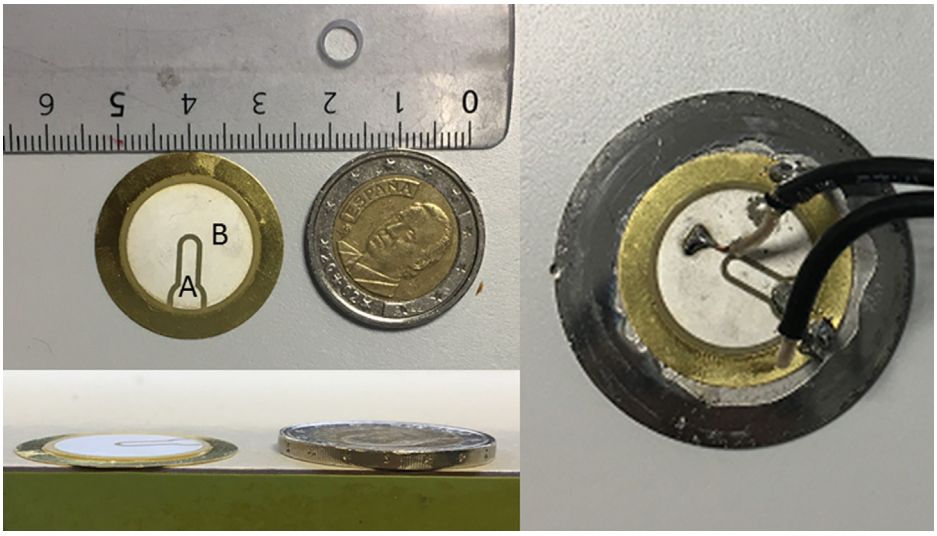

Fig. 5. Piezoelectric transducer consisting of two parts: Receiver (A); Source (B);

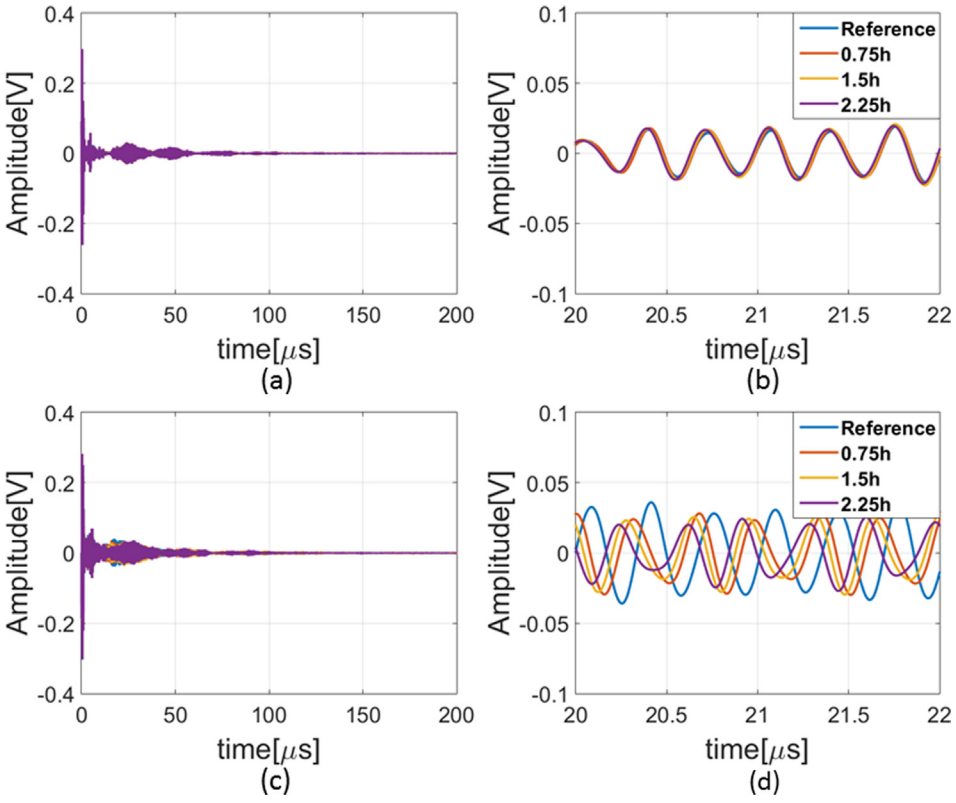

Fig. 6. Measurement signals with a 2 MHz – 5 MHz filter: entire signals of control sample (a); signals of control sample over the interval (20–20.5 μs) (b); entire signals of wax cleaning process (c); signals of wax cleaning process over the interval (20–20.5 μs) (d). The lines with different colors are the results acquired at different moments during the measurement. Blue: reference state; Red: measured at 0.75 h; Yellow: measured at 1.5 h; Purple: measured at 2.25 h.

started recording the data measured by the sensors. Sensor 2 was used to monitor the wax cleaning process. Sensor 1 recorded the data at another position without wax located upstream in the duct, which served as the control. The delay between two acquisitions was 15 s.

2.2.3. *The wax cleaning process*

The entire measurement sequence lasted for about 3 h. During the measurement, two thermometers monitored the water temperature at the inlet and outlet of the duct. There was a slight drop in temperature at the beginning, but it stabilized at 70 °C after 15 min. During that time, a lot of air was exhausted from the duct, which could have a negative effect on the measurement. Therefore, to ensure neither the temperature nor the air had an influence, the acquisitions at the beginning of the measurement were ignored. After acquisition, the circulation of the hot water was stopped and the duct was opened to visually confirm the result of the wax cleaning process. After each cleaning sequence, it was observed that the piece of wax on the inner surface had indeed disappeared.

In order to obtain further information on the dynamics of the wax cleaning, additional cleaning cycles were performed after replacing the stainless steel top plate of the duct with a transparent glass plate of similar dimensions. A video of the cleaning sequence was captured and the images were processed. In the video, it appeared that the wax had totally disappeared after about 2.2 h.

After cooling down the circulating water, the wax dispersed in the water could be observed. This observation was expected as the cleaning process with hot water had progressively melted the wax in the duct, which then solidified as the water temperature decreased.

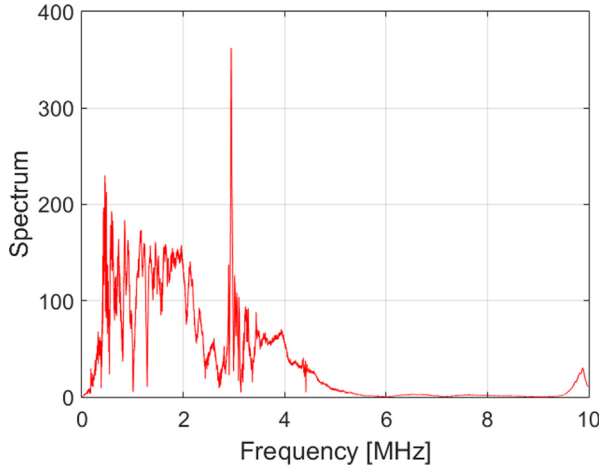

Fig. 7. Spectrum of signals received between 0 MHz and 10 MHz.

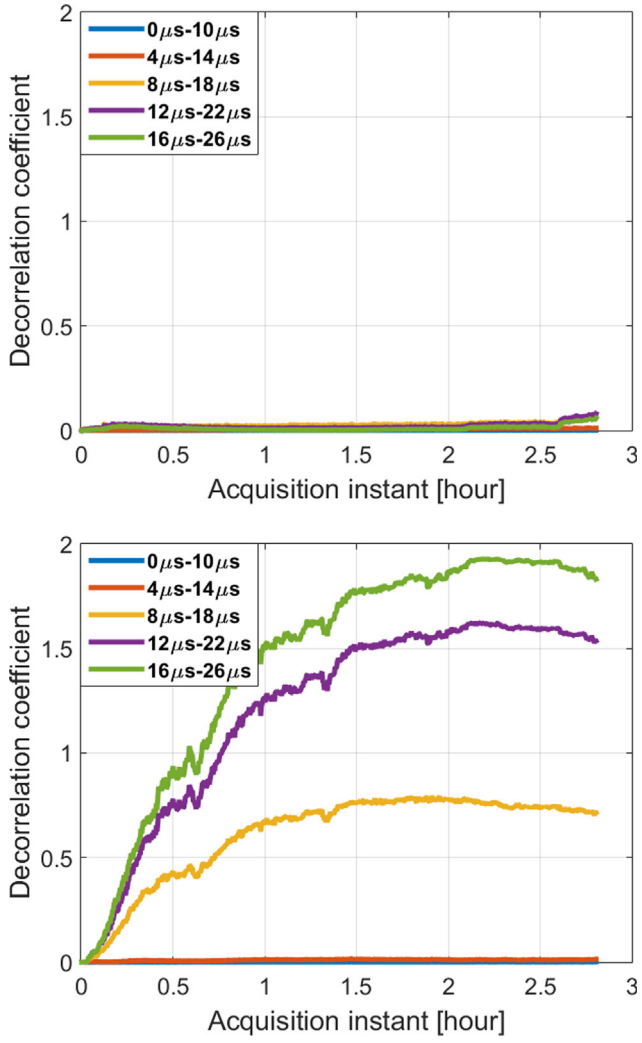

Fig. 8. Decorrelation coefficients: control sample (top) and wax cleaning process (bottom); The different colors represent the decorrelation coefficients of the signals within different windows. Blue: 0–10 μs; Red: 4–14 μs; Yellow: 8–18 μs; Purple: 12–22 μs; Green: 16–26 μs; The sensitivity of the decorrelation coefficient depends on the window. The later the signal used, the higher the sensitivity of the result.

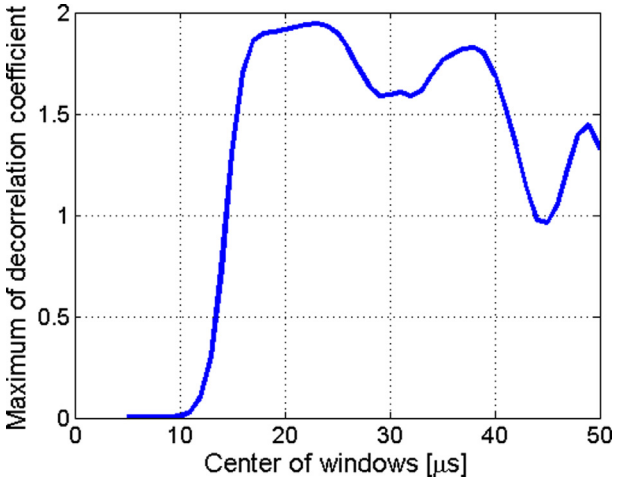

Fig. 9. The stable value (maximum value) of the decorrelation coefficient as a function of the center of the windows. The windows are always 10 μs wide.

3. Results and discussion

3.1. Ultrasonic signal acquisition

Fig. s 6-(a) and (c) show typical echograms received by sensors 1 and 2, respectively. Sensor 2 was located on the upper side of the surface fouled with wax while sensor 1 (control) was placed on the upper side of a clean surface.

For both sensors (Fig. 6-(a) and (c)), it could be observed that the signal amplitudes of the direct waves were rapidly attenuated whereas the attenuation of the signal was more progressive for the coda waves.

The signals in the time window [20–22 μs] are presented for both sensors (Fig. 6-(b) for sensor 1 and Fig. 6-(d) for sensor 2), which shows the coda wave signals in more detail. Each colored curve in Fig. 6-(b) and Fig. 6-(d) corresponds to an echogram obtained after a different period in the cleaning cycle: 0 h (immediately after starting signal acquisition), 0.75 h, 1.5 h, and 2.25 h. The signal to noise ratio at [20–22 μs] was about 30 dB, which was good enough for the analysis. Here, an average of 10 signals measured continuously was used to reduce the noise level for all the other signals recorded.

For sensor 2 (Fig. 6-(d)), the signal varied in both amplitude and time shift according to the stage of the cleaning protocol.

For sensor 1 (control), regardless of the period in the cleaning cycle, the signals looked very similar and could be superimposed. This trend was expected, as sensor 1 was placed on the upper side of a clean surface, the state of which was not supposed to change during the cleaning protocol. This result illustrates the fact that coda wave interferometry can show any change in the state of the sample, provided there are no other perturbations in the acoustic propagation field (temperature variation, flux variation, loud noise…).

For all the graphs in Fig. 6, the sinusoid period of the source signal was 3 MHz. The aim of the band-pass filter was to adjust the sensitivity to the specific conditions and reduce the influence of noise. As the emission signal was a single sinus period, its spectrum was wide band. However, in the spectrum of signals received (Fig. 7), there was only a narrow peak at 3 MHz, which is the excitation frequency. The high-frequency bound of 5 MHz simply corresponds to the highest frequency in the received signal spectrum. The lower bound of the band-pass filter (2 MHz) was selected so that the central excitation frequency was 3 MHz. In addition, after testing several frequencies, the optimum decorrelation sensitivity was obtained for the band [2–5 MHz].

3.2. The decorrelation coefficient with and without wax

The decorrelation coefficient was used as an indicator to quantify

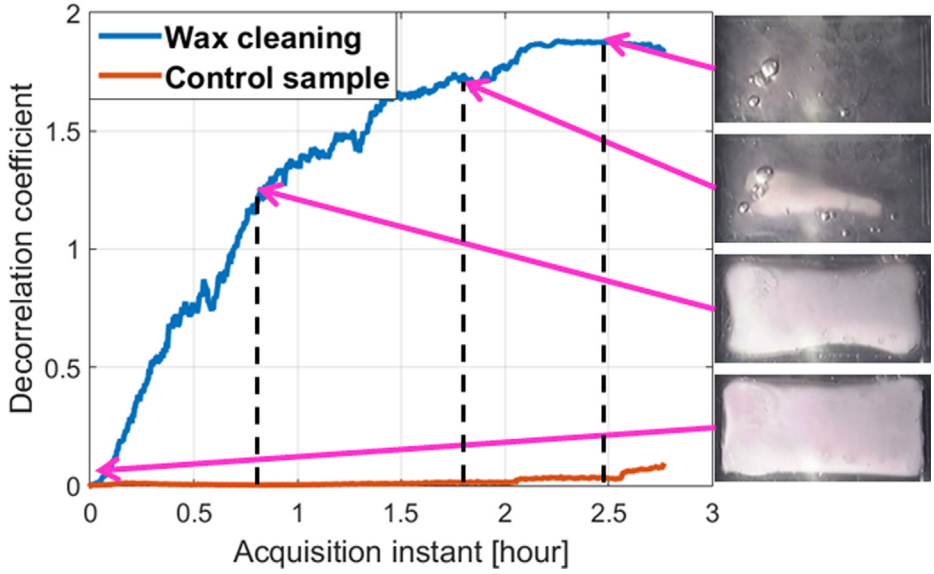

Fig. 10. Decorrelation coefficient curves: control sample (red) and wax cleaning process (blue) for the window 16–26 μs. Photo of wax at different moments (right, from bottom to top): reference state, state at 0.8 h, state at 1.8 h, state at 2.5 h.

the evolution in fouling compared to a reference state. As highlighted before, the decorrelation coefficient provides a global overview of the dissimilarity between two signals. Here, the dissimilarity between the coda signals measured at time t and the initial state (fouled state) was computed and served as an indicator of fouling. In this work, 720 signals were recorded over about 2.75 h, which corresponds to the duration of the cleaning protocol.

Only part of the coda signals was used to compute the decorrelation coefficients. Hence, five different time-domain windows 10 μs wide were tested ([0–10 μs], [4–14 μs], [8–18 μs], [12–22 μs], [16–26 μs]) to find out which parts of the echogram were more sensitive to the degree of fouling. In our case, the width of the time window was 30 times the excitation signal period and the chosen band-pass filter was such that $\Delta f \cdot \Delta t > > 1$, which fully satisfies the conditions mentioned in Section 2.1.2. Fig. 8 shows the evolution of the decorrelation coefficient for sensors 1 and 2 for the five different time-domain windows.

For sensor 2, the evolution of the decorrelation coefficient depended on the time-domain window used for the analysis. For the last three time-domain windows ([8–18 μs], [12–22 μs], [16–26 μs]), a drastic increase in the decorrelation coefficient with cleaning time was observed, then a plateau was reached. This increase in the decorrelation coefficient was correlated to the decrease in wax fouling. Furthermore, the fact that at that time the substrate surface was almost clean and all the wax in the duct had been washed away could explain the plateau.

Conversely, for the first two time-domain windows chosen ([0–10 μs], [4–14 μs]), no increase in the decorrelation coefficient was observed during the cleaning process.

Theoretically, the sensitivity of different parts of the coda waves varies because of differences in overall propagation distance in the specimen. In our case, it is clear that the time-domain window [16–26 μs] was more sensitive and likely to inform us of any change in fouling state. Conversely, the first two time-domain windows ([0–10 μs], [4–14 μs]) were not suitable for detecting any change in fouling state.

For the first two time-domain windows chosen ([0–10 μs], [4–14 μs]), the signals analyzed were very similar to the direct waves, so it is logical that the sensitivity was not remarkable and that the decorrelation coefficient did not evolve.

For sensor 1 (control), the decorrelation coefficient was relatively stable whatever the time-domain window, as expected.

The window selection corresponds to a compromise between sensitivity and signal-to-noise ratio. Indeed, the latter parts of the coda should theoretically correspond to a better decorrelation sensitivity. However, since the amplitudes are lower, the SNR is lower too, resulting in a mitigation of the sensitivity gain when using later coda windows. Fig. 9 shows the sensitivities of the different parts of the signals. The width of the windows was 10 μs. The center of the windows shifts from 5 μs to 45 μs. The maximum decorrelation coefficient after 2.25 h was chosen as an indicator of sensitivity. From Fig. 9, it appears that the time window [16–26 μs] corresponds to the best compromise. The oscillation of the maximum value after 20 μs comes from the narrow peak at 3 MHz in the spectrum (Fig. 7), which implies some periodicity in the received signals, and the decrease in the SNR, as explained above.

Hence, the decorrelation coefficients for sensors 1 and 2 have been plotted simultaneously on the same graph (Fig. 10) using the time-domain window [16–26 μs].

In addition, several pictures extracted from the video at different times during the cleaning process are also presented to show the evolution in fouling over time. These pictures confirm that the evolution of the decorrelation coefficient is directly related to the state of cleanliness.

Of course, it was not possible to ascertain that the two cleaning processes for the two similar ducts were rigorously identical, as the adhesion properties of wax on glass and on stainless steel plates could be different. In addition, slight variations in flow could have led to differences in the elimination process of the wax. However, the digital images obtained with the transparent duct are still pertinent and give an idea of the evolution of fouling over time.

Fig. 10 clearly illustrates the capacity of the proposed monitoring tool to capture the evolution of the fouling state.

4. Conclusion

In this paper, an ultrasonic method based on Coda Wave Interferometry for monitoring the cleaning of fouling deposits on stainless steel ducts is presented. This method shows that the evolution of fouling can be captured non-invasively in an opaque channel.

Two sensors were installed to ascertain the feasibility of this innovative method, presented here for the first time. Sensor 2 was used to monitor the wax cleaning process, while sensor 1 was used as a control, with no wax deposit in the detection area.

The decorrelation coefficient was used as an indicator of a change in the acoustic signal during the cleaning process. The variation in the decorrelation coefficients obtained with the control and during cleaning is clear. A valuable advantage of this method is the capacity to adjust the sensitivity. Indeed, both the band-pass filter and the time-domain window chosen for the analysis have a direct influence on sensitivity. By adjusting these parameters, the correct sensitivity to achieve accurate detection according to the conditions can be obtained. Moreover, there are no critical requirements concerning the quality of the sensors. Hence, the cost would be low.

In future research, the suitability of the method to follow the formation of biofilms and the elimination of whey protein deposits in the dairy industry will be addressed.

Acknowledgments

This research was funded by the Hauts-de-France Region and the University of Valenciennes and Hainaut-Cambresis (UVHC). The work was carried out at the IEMN-DOAE (Institute of Electronics, Microelectronics and Nanotechnology - Department of Opto-Acousto-Electronics) in collaboration with INRA (National Institute for Agricultural Research).

Appendix A. Supplementary material

Supplementary data to this article can be found online at https://doi.org/10.1016/j.ultras.2018.12.011.

References

[1] J. Taborek, T. Aoki, R.B. Ritter, J.W. Palen, J.G. Knudsen, Fouling: the major unresolved problem in heat transfer, (1972).
[2] P. Marty, Maîtrise de la consommation d'eau dans les industries agro-alimentaires: Dossier eau, Ind. Aliment. Agric. 118 (5) (2001) 35–39.
[3] A.J. Van Asselt, M.M.M. Vissers, F. Smit, P. De Jong, In-line control of fouling, Proceedings of Heat Exchanger Fouling and Cleaning-Challenges and Opportunities, Engineering Conferences International, Kloster Irsee, (2005).
[4] P.J. Fryer, G.K. Christian, W. Liu, How hygiene happens: physics and chemistry of cleaning, Int. J. Dairy Technol. 59 (2) (May 2006) 76–84.
[5] N. Alvarez, G. Daufin, G. Gésan-Guiziou, Recommendations for rationalizing cleaning-in-place in the dairy industry: Case study of an ultra-high temperature heat exchanger, J. Dairy Sci. 93 (2) (Feb. 2010) 808–821.
[6] H. Martin, The generalized Lévêque equation and its practical use for the prediction of heat and mass transfer rates from pressure drop, Chem. Eng. Sci. 57 (16) (Aug. 2002) 3217–3223.
[7] E. Wallhäußer, M.A. Hussein, T. Becker, Detection methods of fouling in heat exchangers in the food industry, Food Control 27 (1) (Sep. 2012) 1–10.
[8] R. Guérin, G. Ronse, L. Bouvier, P. Debreyne, G. Delaplace, Structure and rate of growth of whey protein deposit from in situ electrical conductivity during fouling in a plate heat exchanger, Chem. Eng. Sci. 62 (7) (Apr. 2007) 1948–1957.
[9] M. Khaldi, et al., Effect of the calcium/protein molar ratio on β-lactoglobulin denaturation kinetics and fouling phenomena, Int. Dairy J. 78 (Mar. 2018) 1–10.
[10] T.J. Davies, S.C. Henstridge, C.R. Gillham, D.I. Wilson, Investigation of whey protein deposit properties using heat flux sensors, Food Bioprod. Process 75 (2) (Jun. 1997) 106–110.
[11] T. Truong, S. Anema, K. Kirkpatrick, H. Chen, The use of a heat flux sensor for in-line monitoring of fouling of non-heated surfaces, Food Bioprod. Process 80 (4) (Dec. 2002) 260–269.
[12] G. Delaplace, J.-F. Demeyre, R. Guérin, P. Debreyne, J.-C. Leuliet, Determination of representative and instantaneous process side heat transfer coefficients in agitated vessel using heat flux sensors, Chem. Eng. Process. Process Intensif. 44 (9) (Sep. 2005) 993–998.
[13] J.Y.M. Chew, W.R. Paterson, D.I. Wilson, Fluid dynamic gauging for measuring the strength of soft deposits, J. Food Eng. 65 (2) (Nov. 2004) 175–187.
[14] Y.M.J. Chew, W.R. Paterson, D.I. Wilson, Fluid dynamic gauging: a new technique for studying membrane fouling, Water Sci. Technol. Water Supply 7 (5–6) (Dec. 2007) 175.
[15] P.M. Withers, Ultrasonic, acoustic and optical techniques for the non-invasive detection of fouling in food processing equipment, Trends Food Sci. Technol. 7 (9) (Sep. 1996) 293–298.
[16] N. Collier, Développement d'un outil ultrasonore de caractérisation des propriétés d'adhésion de milieux modèles avec application aux dépôts laitiers, Lille 1 (2014).
[17] C. Modin, et al., QCM-D studies of attachment and differential spreading of pre-osteoblastic cells on Ta and Cr surfaces, Biomaterials 27 (8) (Mar. 2006) 1346–1354.
[18] J.J. da Silva, M.G. Wanzeller, P. de A. Farias, J.S. da R. Neto,, Development of circuits for excitation and reception in ultrasonic transducers for generation of guided waves in hollow cylinders for fouling detection, IEEE Trans. Instrum. Meas. 57 (6) (2008) 1149–1153 Jun..
[19] T.R. Hay, J.L. Rose, Fouling detection in the food industry using ultrasonic guided waves, Food Control 14 (7) (Oct. 2003) 481–488.
[20] K.R. Lohr, J.L. Rose, Ultrasonic guided wave and acoustic impact methods for pipe fouling detection, J. Food Eng. 56 (4) (Mar. 2003) 315–324.
[21] B. Merheb, G. Nassar, B. Nongaillard, G. Delaplace, J.C. Leuliet, Design and performance of a low-frequency non-intrusive acoustic technique for monitoring fouling in plate heat exchangers, J. Food Eng. 82 (4) (Oct. 2007) 518–527.
[22] A. Pereira, R. Rosmaninho, J. Mendes, L.F. Melo, Monitoring deposit build-up using a novel mechatronic surface sensor (MSS), Food Bioprod. Process 84 (4) (Dec. 2006) 366–370.
[23] R. Teixeira, A. Pereira, J. Mendes, L.F. Melo, Identifying the nature of fouling layers by online monitoring of the propagation of vibrations along the deposition surface, Heat Transf. Eng. 35 (3) (Feb. 2014) 251–257.
[24] S. Persin, B. Tovornik, Real-time implementation of fault diagnosis to a heat exchanger, Control Eng. Pract. 13 (8) (Aug. 2005) 1061–1069.
[25] G.R. Jonsson, S. Lalot, O.P. Palsson, B. Desmet, Use of extended Kalman filtering in detecting fouling in heat exchangers, Int. J. Heat Mass Transf. 50 (13) (Jul. 2007) 2643–2655.
[26] F. Delmotte, S. Delrot, S. Lalot, M. Dambrine, Fouling detection in heat exchangers with fuzzy models, Proceedings of the 19th International Symposium on Transport Phenomena, Iceland, (2008).
[27] G. Mercere, H. Palsson, T. Poinot, Continuous-time linear parameter-varying identification of a cross flow heat exchanger: a local approach, IEEE Trans. Control Syst. Technol. 19 (1) (Jan. 2011) 64–76.
[28] S. Lalot, G. Mercère, Detection of fouling in a heat exchanger using a recursive subspace identification algorithm, Proceedings of the 19th International Symposium on Transport Phenomena, 2008, pp. 17–21.
[29] S. Lalot, H. Pálsson, Detection of fouling in a cross-flow heat exchanger using a neural network based technique, Int. J. Therm. Sci. 49 (4) (Apr. 2010) 675–679.
[30] K. Aki, B. Chouet, Origin of coda waves: Source, attenuation, and scattering effects, J. Geophys. Res. 80 (23) (Aug. 1975) 3322–3342.
[31] R. Snieder, The theory of Coda Wave interferometry, Pure Appl. Geophys. 163 (2–3) (Mar. 2006) 455–473.
[32] A.A. Grêt, Time-lapse monitoring with Coda Wave interferometry, Colorado School of Mines (2004).
[33] R. Snieder, Coda wave interferometry for estimating nonlinear behavior in seismic velocity, Science 295 (5563) (Mar. 2002) 2253–2255.
[34] R. Zhou, L. Huang, J.T. Rutledge, M. Fehler, T.M. Daley, E.L. Majer, Coda-wave interferometry analysis of time-lapse VSP data for monitoring geological carbon sequestration, Int. J. Greenh. Gas Control 4 (4) (Jul. 2010) 679–686.
[35] A. Ratdomopurbo, G. Poupinet, Monitoring a temporal change of seismic velocity in a volcano: application to the 1992 eruption of Mt. Merapi (Indonesia), Geophys. Res. Lett. 22 (7) (Apr. 1995) 775–778.
[36] S. Matsumoto, K. Obara, K. Yoshimoto, T. Saito, A. Ito, A. Hasegawa, Temporal change in P-wave scatterer distribution associated with the M6.1 earthquake near Iwate volcano, northeastern Japan, Geophys. J. Int. 145 (1) (Apr. 2001) 48–58.
[37] Y. Zhang, Contrôle de santé des matériaux et structures par analyse de la coda ultrasonore, Université du Maine, 2013.
[38] Y. Zhang, et al., Nonlinear mixing of ultrasonic coda waves with lower frequency-swept pump waves for a global detection of defects in multiple scattering media, J. Appl. Phys. 113 (6) (2013) 064905.
[39] B. Hilloulin, et al., Small crack detection in cementitious materials using nonlinear Coda Wave modulation, NDT E Int. 68 (Dec. 2014) 98–104.
[40] T. Planès, E. Larose, A review of ultrasonic Coda Wave Interferometry in concrete, Cem. Concr. Res. 53 (Nov. 2013) 248–255.
[41] S.C. Stähler, C. Sens-Schönfelder, E. Niederleithinger, Monitoring stress changes in a concrete bridge with coda wave interferometry, J. Acoust. Soc. Am. 129 (4) (Apr. 2011) 1945–1952.
[42] C. Payan, V. Garnier, J. Moysan, P.A. Johnson, Determination of third order elastic constants in a complex solid applying Coda Wave interferometry, Appl. Phys. Lett. 94 (1) (Jan. 2009) 011904.
[43] R. Snieder, Extracting the Green's function from the correlation of coda waves: a derivation based on stationary phase, Phys. Rev. E 69 (4) (Apr. 2004) 046610.